The ISME Journal (2014) 8, 52–62

www.nature.com/ismej

ORIGINAL ARTICLE

Physiologic and metagenomic attributes of the rhodoliths forming the largest $CaCO_3$ bed in the South Atlantic Ocean

Giselle S Cavalcanti[1], Gustavo B Gregoracci[1], Eidy O dos Santos[1], Cynthia B Silveira[1], Pedro M Meirelles[1], Leila Longo[2], Kazuyoshi Gotoh[3], Shota Nakamura[3], Tetsuya Iida[3], Tomoo Sawabe[4], Carlos E Rezende[5], Ronaldo B Francini-Filho[6], Rodrigo L Moura[1], Gilberto M Amado-Filho[2] and Fabiano L Thompson[1]

[1]*Institute of Biology, Federal University of Rio de Janeiro (UFRJ), Rio de Janeiro, Brazil;* [2]*Instituto de Pesquisas Jardim Botânico do Rio de Janeiro, Rio de Janeiro, Brazil;* [3]*Laboratory of Genomic Research on Pathogenic Bacteria, International Research Center for Infectious Diseases, Research Institute for Microbial Diseases, Osaka University, Osaka, Japan;* [4]*Laboratory of Microbiology, Hokkaido University, Sapporo, Japan;* [5]*Environmental Science Laboratory, Campos dos Goytacazes, UENF, Rio de Janeiro, Brazil and* [6]*Department of Engineering and Environment, Federal University of Paraíba, Paraíba, Brazil*

Rhodoliths are free-living coralline algae (*Rhodophyta*, *Corallinales*) that are ecologically important for the functioning of marine environments. They form extensive beds distributed worldwide, providing a habitat and nursery for benthic organisms and space for fisheries, and are an important source of calcium carbonate. The Abrolhos Bank, off eastern Brazil, harbors the world's largest continuous rhodolith bed (of $\sim$21 000 km^2) and has one of the largest marine $CaCO_3$ deposits (producing 25 megatons of $CaCO_3$ per year). Nevertheless, there is a lack of information about the microbial diversity, photosynthetic potential and ecological interactions within the rhodolith holobiont. Herein, we performed an ecophysiologic and metagenomic analysis of the Abrolhos rhodoliths to understand their microbial composition and functional components. Rhodoliths contained a specific microbiome that displayed a significant enrichment in aerobic ammonia-oxidizing betaproteobacteria and dissimilative sulfate-reducing deltaproteobacteria. We also observed a significant contribution of bacterial guilds (that is, photolithoautotrophs, anaerobic heterotrophs, sulfide oxidizers, anoxygenic phototrophs and methanogens) in the rhodolith metagenome, suggested to have important roles in biomineralization. The increased hits in aromatic compounds, fatty acid and secondary metabolism subsystems hint at an important chemically mediated interaction in which a functional job partition among eukaryal, archaeal and bacterial groups allows the rhodolith holobiont to thrive in the global ocean. High rates of photosynthesis were measured for Abrolhos rhodoliths (52.16 μmol carbon m^{-2} s^{-1}), allowing the entire Abrolhos rhodolith bed to produce 5.65 $\times$ 10^5 tons C per day. This estimate illustrates the great importance of the Abrolhos rhodolith beds for dissolved carbon production in the South Atlantic Ocean.

The ISME Journal (2014) **8,** 52–62; doi:10.1038/ismej.2013.133; published online 29 August 2013
Subject Category: Microbe-microbe and microbe-host interactions
Keywords: rhodoliths; holobionts; carbon cycle; biomineralization; Abrolhos Bank

Introduction

Eukaryote–microbe associations are increasingly recognized as being essential for eukaryotic host health and metabolism, enabling the expansion of their physiologic capacities (Rosenberg *et al.,* 2007). The term *holobiont* refers to any organism and all of its associated symbiotic microbes (parasites, mutualists, synergists and amensals) (Rosenberg and Zilber-Rosenberg, 2011), including endobionts and epibionts that perform diverse ecological roles (Wahl *et al.,* 2012). A holobiont occupies and adapts to an ecological niche, and is able to employ strategies unavailable in any one species alone when challenged by environmental perturbations. The holobiont concept, first applied to corals after they were found to host abundant and species-specific microbial communities (Rohwer *et al.,* 2002; Reshef *et al.,* 2006; Rosenberg *et al.,* 2007),

Correspondence: FL Thompson, Av. Carlos Chagas Fo. S/N—CCS—IB—BIOMAR—Lab de Microbiologia—BLOCO A (Anexo) A3—sl 102, Cidade Universitária, Rio de Janeiro CEP 21941-599, RJ, Brazil.
E-mail: fabiano.thompson@biologia.ufrj.br
Received 25 March 2013; revised 23 June 2013; accepted 4 July 2013; published online 29 August 2013

has since been extended to the benthic alga (Barott *et al.,* 2011). These holobionts are diverse and distinct from the microbiota in the surrounding seawater and biofilms on abiotic surfaces (Barott *et al.,* 2011; Burke *et al.,* 2011; Barott and Rohwer, 2012). A wide range of beneficial and detrimental interactions have been described between macroalgae and their microbiomes based on the exchange of nutrients, minerals and secondary metabolites (Hollants *et al.,* 2012).

Rhodoliths are biogenic calcareous structures primarily formed by encrusting coralline algae (CCA; *Corallinales, Rhodophyta*). They provide highly biodiverse and heterogeneous habitats and are distributed worldwide (Foster, 2001; Steller *et al.,* 2003; Nelson, 2009). Despite our vast knowledge concerning the ecophysiology and biogeography of rhodoliths, some aspects of the biology of rhodoliths remain completely unknown. For instance, information on the microbial communities, the microbial metabolic strategies associated with biogeochemical cycles and the biomineralization of $CaCO_3$, and the photosynthetic productivity potential of rhodoliths is absent.

Rhodolith beds constitute one of the Earth's four major macrophyte-dominated benthic communities, along with kelp beds, seagrass meadows and coralline algal reefs. Our group has mapped the largest rhodolith bed in the world, which covers $\sim$20 900 km^2 of the Abrolhos Shelf (16°50′–19°45′S) (Amado-Filho *et al.,* 2012). The Abrolhos Bank is one of the largest marine $CaCO_3$ deposits in the world, with a production of 25 megatons of $CaCO_3$ per year (Amado-Filho *et al.,* 2012). Nevertheless, our limited knowledge of rhodolith biology hinders our ability to develop a broader systemic understanding of their ecological role in the Abrolhos Bank. There are pressing concerns relating to the future of rhodolith beds as global carbon budgets, and ocean acidification may interfere with rhodolith functioning and biogeochemical stability (Webster *et al.,* 2011; Whalan *et al.,* 2012). In addition, because rhodoliths can be applied agriculturally to improve soil pH, rhodolith environments have been suffering extensive commercial pressure. In addition, rhodoliths are a non-renewable resource because of their extremely slow growth rates (Dias, 2001; Barbera *et al.,* 2003; Wilson *et al.,* 2004).

Rhodoliths form biogenic matrices with complex structures in which the interlocking branched thalli can create microhabitats for diverse eukaryotic assemblages, including epiphyte algae, microalgae and different types of invertebrates from both hard and soft benthos (Steller *et al.,* 2003; Kamenos *et al.,* 2004; Figueiredo *et al.,* 2007; Riul *et al.,* 2009; Bahia *et al.,* 2010). Owing to the rich three-dimensional architecture, each rhodolith holobiont may be considered a small individual reef, providing a habitat for the young of various types of marine life (for example, Arthropoda, Nematoda and Cnidaria). Habitat and nursery functions are the most obvious ecological roles that rhodoliths have in the marine realm. Rhodoliths may be key factors in a range of invertebrate-recruitment processes, functioning as autogenic ecosystem engineers by providing three-dimensional habitat structures. A better understanding of the composition of and ecological interactions within the rhodolith holobiont would be a powerful tool for the conservation and sustainable use of these biological resources. This understanding could also provide insights into how cooperation and job partitioning between constituents contribute to holobiont fitness, influence holobiont viability, and consequently affect associated ecosystems and the ubiquitous rhodolith worldwide distribution. We aimed to perform a metagenomic characterization of the Abrolhos rhodoliths to determine the major taxonomic and functional components of these organisms. We also examined the associated fauna diversity and physiologic aspects (photosynthetic capacity and dissolved organic carbon (DOC) productivity) of the rhodoliths.

Materials and methods

Study site and sample collection

This study was carried out in the Abrolhos Shelf off eastern Brazil. Rhodoliths were collected by scuba diving in December 2010 from three different sites near two recently described sinkhole-like structures called *Buracas* (Bastos *et al.,* 2013). *Buracas* are cup-shaped depressions on the seafloor and their suggested function is to trap and accumulate organic matter, thus functioning as productivity hotspots in the mid- and outer shelf of the central portion of the Abrolhos Bank (Cavalcanti *et al.,* 2013). Seven rhodoliths were sampled as follows: two individual rhodoliths from the shallower portion (27 m) (17.81330° S/38.23744° W) outside the first *Buraca*; three from the inner region of the same *Buraca* (43 m deep) (17.81399° S/38.24306° W) and two from a deeper point (51 m) (17.91361° S/37.90936° W) near another sinkhole-like structure (Supplementary Table S1) away from the first (Figure 1). Monospecific rhodolith-forming CCA were selected by visual inspection. Immediately after collection, the specimens were frozen in liquid nitrogen in the field. For comparison purposes, surrounding water samples (8 l) collected using sterivex 0.2-μm filters at exactly the same points over the rhodolith beds at the first *Buraca* (inside—43 m; outside—27 m) and outside the deeper *Buraca* (51 m) were used. A detailed description of the region of the *Buracas*, water sampling and metagenomic characterization of the planktonic microbial community is available in the work by Cavalcanti *et al.* (2013).

DNA extraction, pyrosequencing and sequence analysis

In the laboratory, a small fragment of each rhodolith sample ($\sim$1 cm^2) was sterilely macerated with liquid

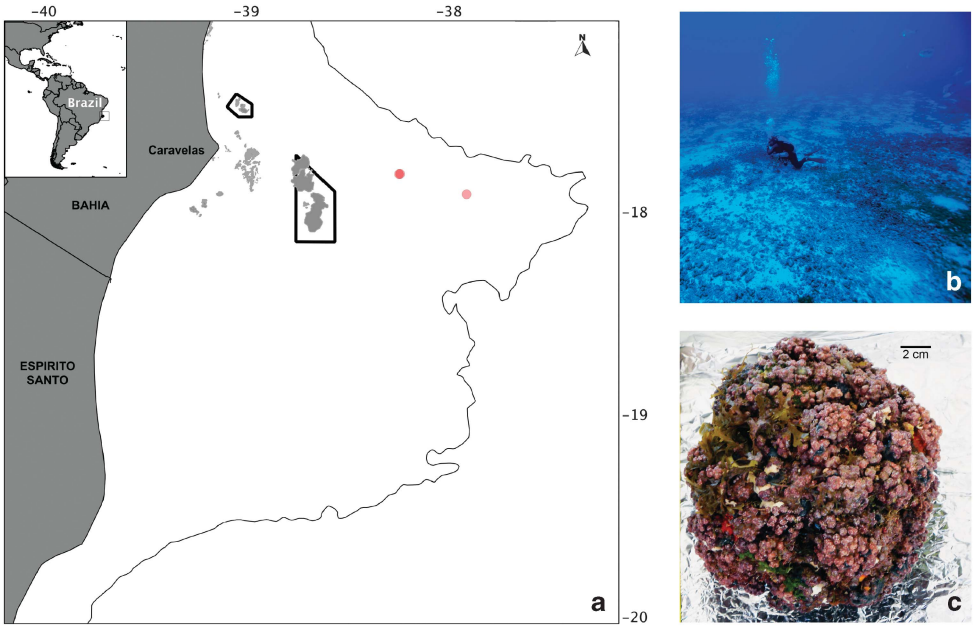

Figure 1 Study site. The world's largest rhodolith bed. (**a**) The Abrolhos bank, an expanse covering ~46 000 km^2 of the eastern Brazilian continental shelf where the rhodolith bed covers an area of ~21 000 km^2. Rhodoliths were sampled from two different sites surrounding the recently described sinkhole-like structures (red dots). (**b**) Physiognomy of Abrolhos rhodolith beds. (**c**) Individual monospecific rhodoliths.

nitrogen without the separation of epibionts to provide a representation of the entire rhodolith holobiont as previously defined (calcifying algae plus associated microbes, fauna and flora). A subsequent step using CTAB buffer with 100 mM of EDTA and a PowerSoil purification column was used to gather the DNA of high-molecular-weight rhodolith holobionts as described by Garcia *et al.* (2013). High-quality total DNA extracted from rhodoliths was then sequenced using a 454 GS Jr machine (454 Life Sciences, Branford, CT, USA) and the GS Jr Titanium-sequencing process. Sequences were submitted to the MG-RAST 3.1 server (Metagenomics-Rapid Annotation Using Subsystems Technology) (Meyer *et al.,* 2008) and quality filtered. Post-quality-control (QC) sequences were annotated using the (SEED) Subsystems Technology for functional classification (Overbeek *et al.,* 2005) and the GenBank database for phylogenetic analyses. All BLAST queries were performed with a maximum expected cutoff value of 10^{-5}.

Statistical analyses

The Statistical Analysis of Metagenomic Profiles (STAMP v.2.0.0) software was used for statistical analysis (Parks and Beiko, 2010). For comparison purposes, rhodolith metagenomes were compared with water metagenomes from the same site (Cavalcanti *et al.,* 2013). The water and rhodolith samples were compared by using a two-sided Welch's *t*-test with 95% confidence intervals calculated by inverting the Welch's test and by using the Benjamin–Hochberg FDR multiple test correction. A principal component analysis was conducted using the STAMP software package to compare the taxonomic grouping based on the taxonomic class contributions of each metagenome from both the rhodolith and the surrounding seawater. To isolate the relative contributions of taxonomic groups within the rhodolith metagenomes, the most abundant groups (*Alphaproteobacteria, Gammaproteobacteria, Eukarya, Betaproteobacteria, Deltaproteobacteria, Actinobacteria, Firmicutes, Bacteroidetes, Cyanobacteria, Planctomycetes, Archaea* and *Others*) were functionally re-annotated using the Workbench tool, and their functions were compared with an analysis of variance using a Tukey–Kramer *post-hoc* test, an eta-squared effect size and a Benjamin–Hochberg multiple test correction. In all these cases, *P*-values of $<5\%$ were considered statistically significant.

Associated fauna analysis

For each sampling point, the fauna associated with the rhodolith was analyzed. These rhodoliths were preserved in 10% formalin, and the faunal organisms were analyzed with regard to the high-level taxonomic groups, such as phylum, class, order and family, when possible using stereomicroscopy.

Primary productivity of rhodoliths

To determine the photosynthetic activity of rhodoliths in the Abrolhos Bank, we applied the pulse-amplitude-modulated method (PAM) that

uses variations in the effective quantum yield of photosystem II as a method to assess the photosynthetic performance of photosystem II (Schereiber *et al.,* 1966). Briefly, the change in fluorescence emitted by chlorophyll before and after the stimulation with a saturating light pulse is used to calculate the effective quantum yield ($\Delta F/Fm'$) (Maxwell and Johnson, 2000). The underwater DIVING PAM (Walz, Germany) was used directly in the field with a red light under ambient light. DIVING PAM measurements took place 33 m deep in rhodolith beds at 1300 hours on 17 August 2011. A total of 58 measurements were taken in 12 different rhodolith specimens—five measurements per specimen. A consistent distance of 1 cm between the fiberoptic sensor and the rhodolith surface was maintained using an adaptation of the DIVING PAM sample holder. The yield ($\Delta F/Fm'$) was measured using a 0.8 period of saturating light (ca. 8000 $\mu mol\, m^{-2}$ per s), and an absorption factor of 0.56 was applied for electron transport rate (ETR) calculations, as previously determined for Rhodophyta (Beer and Axelsson, 2004) ($ETR = \Delta F/Fm' \times PAR \times 0.5 \times 0.56$, where PAR is the photosynthetic active radiation at the sampling site and 0.5 is the factor that accounts for the distribution of electrons between photosystem I and photosystem II). Similarly, the theoretical model of 0.25 mol of O_2 for each mol of electrons was also used in the ETR calculations (Beer and Axelsson, 2004).

Rhodolith dissolved organic carbon release

Incubation experiments were performed to determine the amount of fixed carbon released by the rhodoliths in the form of exudates. Single rhodoliths, ~10 cm in diameter, were randomly collected and placed inside translucent Niskin bottles, which allow photosynthetically active radiation to pass through for light treatment, or inside covered Niskin Bottles (dark) as a control. The treatments and controls were performed in three replicates, and the experiment was repeated twice. Incubation was carried out *in situ* (at a depth of 30 m) for 2 h from 1300 to 1500 hours using water from near the bottom of the seafloor—the same water mass to which rhodoliths are normally exposed. Dissolved organic carbon (DOC) was measured at time 0 and 2 h later, and the variation in DOC concentrations was analyzed. For the DOC measurements, bottled water samples were filtered using pre-combusted (550 °C) Whatman GF/Filters, preserved using 10% H_3PO_4, and stored and refrigerated in amber glass bottles. Samples were further acidified with 2 N HCl and sparged with ultrapure air, and the DOC was determined by high-temperature catalytic oxidation in a Shimadzu TOC 5000 Analyzer (Ovalle *et al.,* 1999).

Results

A total of 60.85 million non-redundant nucleotide bases (Mb) were generated in this study. Approximately 165 000 high-quality metagenome sequences from seven different rhodoliths from three different sampling sites in the outer region of the Abrolhos Bank were obtained. After quality control, each rhodolith metagenome contained between 17 863 and 32 488 reads, in which an average of 24% was classified by MG-RAST taxonomically (a total of 41 051 sequences) and functionally (a total of 39 691 sequences) (Supplementary Table S1). The major contributing domain was *Bacteria* (~83.64%). The contribution of *Archaea* was ~3%, whereas that of the *Eukarya* domain was the most variable, ranging from 6.5 to 27.4% (Supplementary Table S1).

Taxonomic assignment of rhodolith metagenomes

Rhodolith replicates harbor impressive homogenous and characteristic communities of *Bacteria* (Figure 2). When compared with the surrounding seawater

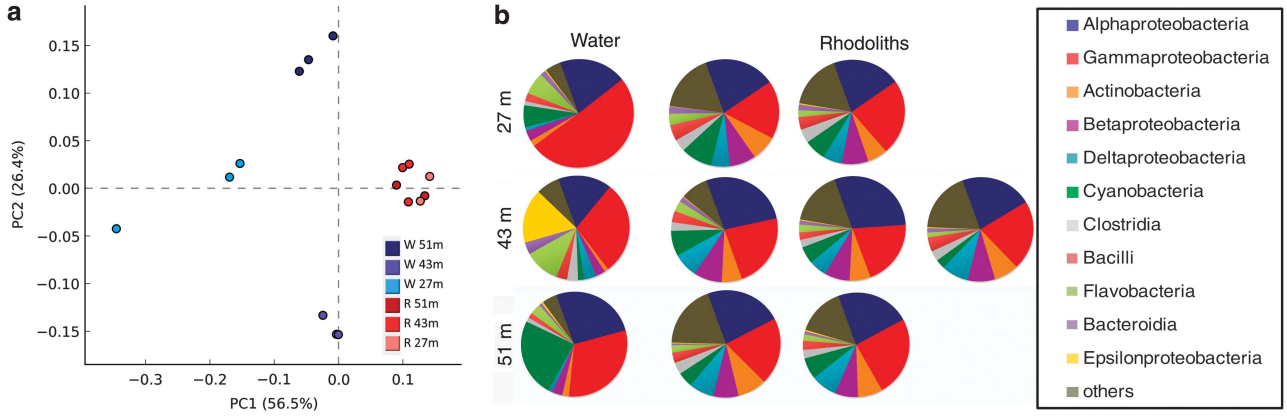

Figure 2 Homogeneity of the rhodolith metagenome. Rhodoliths and the surrounding seawater from depths of 27, 43 and 51 m were compared. (**a**) Principal component analysis (PCA) grouping rhodolith (red) and seawater (blue) metagenomes by class contribution. (**b**) Taxonomic composition of the rhodolith and surrounding water metagenomes. A taxonomic assignment was performed using MG-Rast based on sequence similarities to the GenBank database.

metagenomes, rhodolith metagenomes from different sampling sites clustered closely together based on class-contribution grouping, despite the clustering of surrounding water samples based on site and depth (Figure 2a). The bacterial class composition was extremely consistent among the seven rhodoliths and did not show any site or depth correlations, despite the variability in the surrounding water detailed and discussed by Cavalcanti *et al.* (2013) (Figure 2b). The majority of bacterial sequences were assigned to the Proteobacteria phylum (an average of 47.13%), followed by *Actinobacteria*, *Firmicutes* and *Cyanobacteria*, contributing ~5% each (Figure 3a). The *Alpha*- and *Gammaproteobacteria* together were

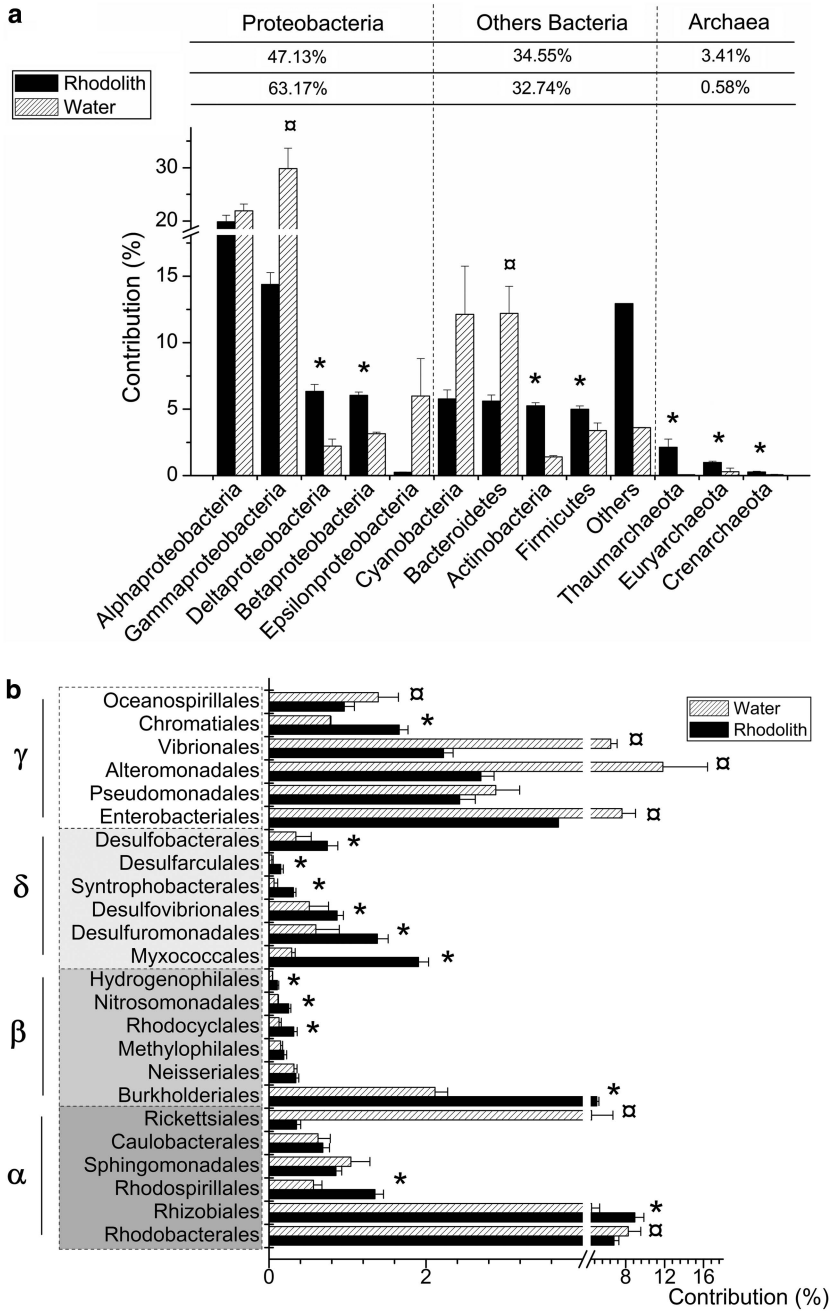

Figure 3 Taxonomic composition of rhodolith metagenomes. A taxonomic assignment was performed using MG-Rast based on sequence similarities to the GenBank database. (**a**) The average percentage of sequences from rhodolith and the surrounding water metagenome with the best BLAST similarity to Archaeal and Bacterial domains (phylum Proteobacteria and other Bacteria phyla). (**b**) More detailed breakdown of the Proteobacteria group. Relative contribution of the main proteobacterial orders in the rhodolith and the surrounding seawater metagenomes. Comparison of taxonomic contributions between rhodoliths and the surrounding water: (*) represents groups that are significantly over-represented in the rhodolith metagenome ($P<0.5$); (¤) represents groups that are significantly over-represented in the seawater metagenome ($P<0.5$).

responsible for 72.65% of the *Proteobacterial* sequences; nevertheless, a significantly greater contribution was observed for *Beta-* and *Deltaproteobacterial* classes relative to the surrounding water. This increased contribution was observed for the majority of orders of *Beta-* and *Deltaproteobacteria*, with a remarkable contribution for *Burkolderiales* (over 5%) (Figure 3b). The other rhodolith-holobiont components, *Archaea* and *Eukarya*, had a more variable constitution between individual rhodoliths. The most abundant archaeal phylum was *Thaumarchaeota* (ranging from 0.48 to 4.12%), with a greater contribution in the samples obtained from deeper water (51 m). In addition to *Thaumarchaeota*, both *Euryarchaeota* and *Crenarchaeota* phyla (a total of 1.26%) were statistically more abundant in the rhodolith metagenomes compared with the surrounding water (Figure 3a). For the *Eukaryota* domain—the most variable domain in our study—over 60% of all the sequences were identified as invertebrate marine phyla *Chordata*, *Arthropoda* and *Cnidaria,* and as algal groups *Streptophyta* and *Chlorophyta* (Supplementary Table S2).

Metabolic diversity of rhodolith metagenomes

The overall functional annotation (subsystems level 1) of rhodoliths was compared with the surrounding water metagenomes (Figure 4). Rhodoliths presented more sequences related to fatty acids, lipids and isoprenoids ($P = 4.38 \times 10^{-2}$), metabolism of aromatic compounds ($P = 7.9 \times 10^{-3}$), secondary metabolism ($P = 4.88 \times 10^{-4}$) and sulfur metabolism ($P = 6.97 \times 10^{-3}$). The water samples had more sequences related to cell division and cell cycle ($P = 3.76 \times 10^{-2}$), iron acquisition and metabolism ($P = 3.31 \times 10^{-2}$), and RNA metabolism ($P = 3.47 \times 10^{-2}$). At the second and third levels, other observed noteworthy differences are listed below, and the rest are summarized in Supplementary Table 3. Briefly, fermentation ($P = 1.92 \times 10^{-2}$)—particularly acetone butanol ethanol (ABE) synthesis ($P = 2.21 \times 10^{-2}$) and butanol biosynthesis ($P = 2.09 \times 10^{-2}$), sulfatases and modifying factors ($P = 8.31 \times 10^{-4}$), fatty acids ($P = 6.24 \times 10^{-3}$), ABC transporters ($P = 3.74 \times 10^{-4}$), metabolism of central aromatic intermediates ($P = 3.27 \times 10^{-2}$), peripheral pathways for the catabolism of aromatic compounds ($P = 3.37 \times 10^{-2}$), biologically active compounds in metazoan cell defense ($P = 2.76 \times 10^{-2}$), steroid sulfates ($P = 2.06 \times 10^{-2}$), galactosylceramide and sulfatide metabolism ($P = 3.05 \times 10^{-3}$), and organic sulfur assimilation ($P = 3.36 \times 10^{-2}$)—was increased in the rhodoliths. Alternatively, DNA replication ($P = 2.73 \times 10^{-3}$), the recBCD DNA repair pathway ($P = 3.97 \times 10^{-2}$), bacterial cell division ($P = 2.84 \times 10^{-2}$), the organic-acid-generating methylcitrate cycle ($P = 3.41 \times 10^{-3}$), and the propionate-CoA to succinate module ($P = 9.34 \times 10^{-3}$), were reduced in the rhodoliths compared with the surrounding water. The comparisons of the most abundant groups revealed distinguishing features. Most metabolic pathways were shared between all the groups, with the following noteworthy exceptions. Potassium metabolism was higher in *Alphaproteobacteria* ($P = 1.15 \times 10^{-5}$). Respiration ($P = 2.77 \times 10^{-3}$) and photosynthesis ($P = 8.46 \times 10^{-7}$) were increased in *Eukarya*, with reasonably large representation in *Archaea* for respiration and in *Cyanobacteria* for photosynthesis. Proteolytic pathways were also more abundant in *Eukarya* ($P = 9.64 \times 10^{-4}$). Iron acquisition and metabolism were more prominent in *Bacteroidetes* ($P = 7.53 \times 10^{-3}$), although *Gammaproteobacteria* were enriched in siderophores ($P = 5.57 \times 10^{-3}$), and *Alphaproteobacteria* had an over-representation of heme and hemin uptake hits ($P = 1.6 \times 10^{-2}$). *Archaea* showed a predominant representation

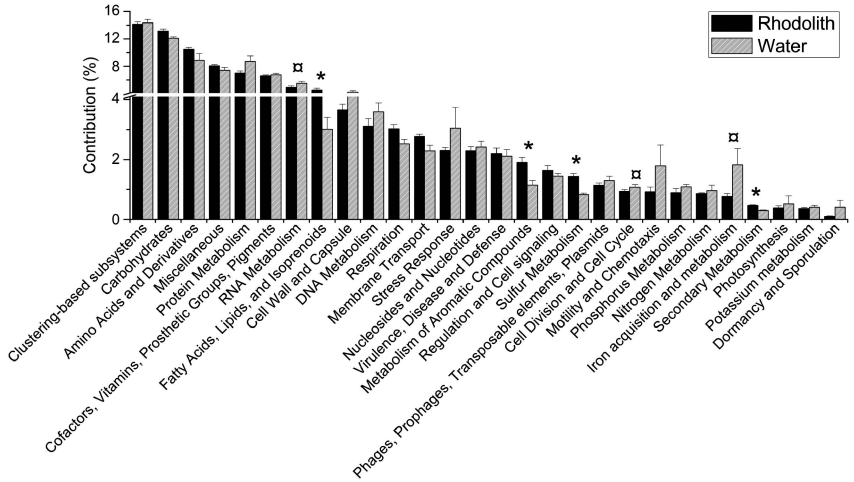

Figure 4 Functional profile. Relative contribution of subsystems (first-level hierarchy) in the rhodolith and surrounding seawater metagenomes. Comparison of functional contributions between rhodoliths and the surrounding water: (*) represents subsystems that are significantly over-represented in the rhodolith metagenome ($P < 0.5$); (¤) represents subsystems that are significantly over-represented in the seawater metagenome ($P < 0.5$).

of several subsystems, including organic acids ($P = 3.3 \times 10^{-2}$), adhesion ($P = 1.86 \times 10^{-5}$), denitrification ($P = 9.91 \times 10^{-3}$) and inorganic sulfur assimilation ($P = 8.71 \times 10^{-7}$), although none of these roles were exclusive to this domain. *Betaproteobacteria* were distinguished by fatty-acid degradation ($P = 7.42 \times 10^{-3}$), and *Deltaproteobacteria* were distinguished by the invasion and intracellular resistance subsystem ($P = 1.3 \times 10^{-2}$). Some groups (*Actinobacteria*, *Bacteroidetes*, *Cyanobacteria* and *Firmicutes*) had higher numbers of DNA repair hits ($P = 3.01 \times 10^{-4}$), but this subsystem was well represented in most bacterial groups. The cAMP signaling was highly represented in *Cyanobacteria* and *Betaproteobacteria* ($P = 1.75 \times 10^{-5}$). Type III protein secretion system orphans ($P = 4.9 \times 10^{-2}$), type IV secretion systems ($P = 9.16 \times 10^{-3}$) and type VIII secretion systems ($P = 4.4 \times 10^{-2}$) were also increased in *Gammaproteobacteria*, *Betaproteobacteria* and *Bacteroidetes*, respectively.

Fauna taxonomic identification

The most frequent taxonomic groups associated with the sampled rhodoliths were the *Foraminiferea, Bryozoa, Annelida* and *Mollusca* phyla, which were observed in all the samples, although represented by different morphotypes. Regarding the epifauna, colonial encrusting forms covered large rhodolith areas, where the most abundant group was *Bryozoa*, followed by *Foraminiferea*, particularly *Homotrema rubrum*. The phylum *Annelida* was largely represented by the encrusting calcareous tubes of *Polychaeta*. The occurrence of the phylum *Mollusca* was observed by the residual shells from *Bivalvia* and *Gastropoda*, particularly from the *Vermetidae* family. The infauna was mainly composed of calcareous tubes of *Polychaeta*, followed by *Bryozoa* and *Foraminiferea*. Different morphotypes (approximately five) of free-living *Foraminiferea* were observed in all the samples, showing the highest species richness compared with the other groups of fauna associated with rhodoliths.

Rhodoliths from the depths of 43 and 51 m showed lower species richness compared with the 27 m sample. Rhodoliths from a depth of 43 m were mainly associated with filamentous green algae, and the sample from this depth was the only containing one specimen and shell marks of *Lithophaga (Bivalvia)*. On the sample from the depth of 51 m, a morphotype of *Brachiopoda* and residuals of *Echinoidea* (Echinodermata) calcareous skeletons were found. The sample from a depth of 27 m presented a different fauna composition from the others, with a large rhodolith surface area covered by colonial forms of *Ascidiacea* (phylum *Chordata*, subphylum *Tunicata*) and *Porifera*, in addition to *Bryozoa*, *Foraminiferea*, *Polychaeta* and *Vermetidae*, completing the epifauna. The most abundant groups, primarily because of their encrusting colonial habits, were *Ascidiacea* and *Porifera*, followed by *Bryozoa* and *Foraminiferea*. In this sample, we observed the occurrence of other groups, including the phyla *Platyhelminthes*, *Nematoda* and *Arthropoda* (subphylum *Crustacea*), and the class *Polyplacophora* (phylum *Mollusca*), although with only one specimen registered for each group.

Primary productivity of rhodoliths

Photosynthetically active radiation from *Lithothamnion crispatum* at a depth of 33 m, the site of measurements, was 1436 ± 47.84 μmol photons $m^{-2} s^{-1}$ (average ± s.e.). The effective quantum yield of photosystem II determined for the rhodoliths ranged from 0.206 to 0.78, with a mean value of 0.511, which allowed linear correlations between ETR and CO_2 fixation. These values were considerably above the 0.1 critical limit value for these correlations. The ETR was 208.67 ± 10.19 μmol electrons $m^{-2} s^{-1}$ (average ± s.e.). Therefore, the calculated CO_2 fixation rate was 52.16 ± 2.57 μmol carbon $m^{-2} s^{-1}$ or 27.03 g carbon m^{-2} per day (Table 1).

Rhodolith organic carbon release

The concentration of DOC in the water just above the rhodolith beds was 1.85 ± 0.32 mg l^{-1} (average ± s.d.). The DOC concentration increased after the 2 h of incubation, with ΔDOC of 0.13 and 0.04 mg l^{-1} for light and dark bottles, respectively. The control bottles had DOC consumptions of 0.26 and 0.28 mg l^{-1} for light and dark bottles, respectively, likely because of the planktonic activity in the Niskin bottles. Discounting the amount of organic carbon consumed by the plankton, we observed that rhodoliths released 0.39 ± 12 and 0.32 ± 19 mg l^{-1} of DOC in light and dark incubations, respectively,

Table 1 Calcifying algae productivity. Photosynthetic capacity of free-living rhodolith holobionts and crustose coralline algae

Organism	*Depth (m)*	*Temperature (°C)*	*Irradiance (μMol photons $m^{-2} s^{-1}$)*	*Fixed carbon (μMol C $m^{-2} s^{-1}$)*	*Reference*
Rhodoliths	33	26	1436 ± 47	52.1 ± 2.5	This study
CCA	6–7	26	9207 ± 907	274.5 ± 36.5	This study
P. foecundum (CCA)	15–18	0–1	<5	45.2–66.9	Roberts *et al.*, 2002
P. tenue (CCA)	15–18	0–1	<5	42.5–47.2	Roberts *et al.*, 2002
M. Engerlhartii (CCA)	16–20	0–1	<5	9.4–17.9	Schwarts *et al.*, 2005

showing no significant difference between these two treatments ($P = 0.8$). The release rate of organic carbon was 0.04 mg ± 0.01 DOC $h^{-1} dm^{-2}$ of rhodolith surface area, or 3.58 ± 1.46 μmol h^{-1} dm^{-2}.

Discussion

Our rhodolith metagenomic analysis demonstrated the wealth of microorganisms that inhabit this holobiont. We verified an extremely similar composition among the microbiomes of the rhodoliths from the three different sampling sites in the Abrolhos Bank—a possible reflection of a long-term host–microbe association. This association may enable the holobiont to expand its physiological capacity and geographic distribution (Hollants *et al.,* 2012). Polychaetes, crustaceans (amphipods), ophiuroids and mollusks, commonly found in the rhodolith infauna of the Abrolhos Bank, were also the main invertebrate taxa inhabiting the rhodoliths analyzed in this study. Our metagenomic analysis extended these previous observations (Figueiredo *et al.,* 2007), detecting other types of flora and fauna (for example, foraminifers).

It is plausible that the genesis and growth of rhodoliths are intimately related to their microbial constituents. The remarkable homogeneity revealed in the rhodolith microbiomes hints at the existence of a close relationship between the microbes and their rhodolith host. Indeed, despite a lack of knowledge of the principles underlying the assembly and the structure of these complex microbial communities, other examples of host specificity have also been illustrated for macroalgal–bacterial interactions (Hollants *et al.,* 2012). Most of the rhodolith metagenomic sequences (over 70%) were identified as bacterial protein-coding sequences. Some bacterial taxa, such as *Alphaproteobacteria*, *Firmicutes* and *Actinobacteria*, are as abundant in the rhodolith holobiont (19.7, 5.8 and 5.8%, respectively) as in other red seaweed–microbe holobionts (13, 10 and 9%, respectively). However, some taxa were particularly enriched in rhodoliths (for example, *Betaproteobacteria* with 6.5% and *Deltaproteobacteria* with 5.7%) compared with other red seaweeds (Hollants *et al.,* 2012). The metabolically diverse groups of the aerobic ammonia-oxidizing betaproteobacteria *Nitrosomonadales, Rodhocyclales* and *Hydrogenophylales*, and the dissimilative sulfate-reducing deltaproteobacteria *Desulfovibrionales, Desulfobacterales* and *Desulforomonadales* were significantly increased in the rhodolith microbiome compared with the surrounding water.

Job partitioning in the rhodolith holobiont

We observed significant contributions of photolithoautotrophs (that is, cyanobacteria (5.09%)), anaerobic heterotrophs (predominantly sulfate-reducing proteobacteria (1.52%)), sulfide oxidizers (0.37%), anoxygenic phototrophs (that is, purple (2.33%) and green sulfur bacteria (1.33%)) and methanogens (0.46%) in the rhodolith metagenome. These guilds with similar metabolic roles operate in collaboration to accomplish the cycling of key elements (O, N, S and C), which may allow them to carry out important tasks, such as biomineralization (Dupraz *et al.,* 2009). Microbially induced carbonate precipitation, which occurs in microbialites, is carried out by the interaction of microbial consortia, their growth and metabolism, cell surface properties, and extracellular polymeric substances (Dupraz *et al.,* 2009). Calcium carbonate formation and precipitation are central processes in rhodolith construction. The corallinaceae algae are considered to be major factors in mineralization in rhodoliths. Comparatively little attention has been paid to the role of rhodolith microbes in calcium carbonate formation and precipitation. Although the diversity and abundance of microbes provide only a cursory indication of what is metabolically feasible, it is noteworthy that in the rhodolith microbiome, we found major functional groups related to microbial-induced organomineralization, which may suggest an important but still unappreciated role of microbes in carbonate precipitation in rhodoliths.

This functional metagenomic profile offers insights into the metabolism of the rhodolith holobiont. Whereas water-column microbes seem more prone to cell division, DNA repair and iron acquisition, rhodolith-associated microbes are more specialized in chemical communication. This interplay is suggested by the increased representation of secondary metabolites, metazoan-active cell compounds and specialized bacterial secretion systems in the rhodolith metagenome. Fatty-acid metabolism and degradation are also important, hinting that an interaction likely occurs in the algal cell membrane. A notable amount of capsular and extracellular polysaccharide hits indicate a structured biofilm in association with this surface. Although the rhodolith biofilm is clearly less impressive than coral mucus or microbial mats, the presence of certain taxonomic groups suggests that a considerable degree of spatial structuring occurs in this biofilm, providing microenvironments that support different metabolic guilds, akin to corals (Garcia *et al.,* 2013), and microbial mats (Dupraz *et al.,* 2009). Interestingly, it has long been known that the cell wall or mucilage is the calcification site in coralline red algae, such as rhodoliths (Borowitzka, 1987), perhaps with an intravesicular stage that could involve the Golgi apparatus (Krumbein and Larkum, 1987). Mineralization in these algae is strictly controlled, as every aspect of the process is regulated by the eukaryotic cell (Borowitzka, 1987; Dupraz *et al.,* 2009). Given this close affinity, it is likely that the microbial composition and metabolic rates associated with this structure will influence its physicochemical characteristics (Dupraz and Visscher, 2005; Dupraz *et al.,* 2009). The promotion (+) or hindrance (−) of calcium carbonate precipitation is

determined by the net effect of competing and antagonistic microbial metabolic processes, which cannot be predicted based only on the functions revealed by metagenomics (Khodadad and Foster, 2012). However, our study revealed interesting features of the rhodolith metagenome. For instance, the main energy production and carbon fixation pathways appear to be via algal photosynthesis (+). *Cyanobacteria* appear to have a secondary role in this system. The main carbon-cycling balance (photosynthesis (+)/respiration(−)) is performed by *Eukarya*, unlike in stromatolites (Dupraz *et al.,* 2009). Microbial metabolism may still have a role in terms of anoxygenic photosynthesis (+), fermentation (−), and aerobic (−) and anaerobic respirations (+) (sulfate reduction, denitrification) (Krumbein and Larkum, 1987; Visscher *et al.,* 1998; Dupraz and Visscher, 2005; Dupraz *et al.,* 2009). Although some organic-acid-generating metabolic pathways (−) are reduced in rhodoliths, the higher representation of fermentation (−), butanol biosynthesis (−) and ABE synthesis (−) suggest a negative role for microbes in rhodolith calcification. However, sulfate oxidizers (+) and anoxygenic photosynthesis (+) guilds were detected in this holobiont and could significantly promote the precipitation of calcium carbonate in the rhodoliths.

Another potential influence of the microbes in rhodoliths is in sulfur cycling, similar to modern marine stromatolites in the Bahamas (Visscher *et al.,* 1998) and Mexico (Breitbart *et al.,* 2009). The negatively charged sulfated polysaccharides of the algal cell wall are likely the ligands for Ca^{2+} ions (Borowitzka, 1987). Theoretically, these polysaccharides can also limit carbonate precipitation by sequestering these ions in the organic matrix (Dupraz *et al.,* 2009). We also observed steroid sulfates. The presence of sulfatases, sulfatide metabolism and organic sulfur assimilation pathways indicates a microbial role in the cleavage and cycling of these sulfur radicals, similar to the model proposed for microbialites (Breitbart *et al.,* 2009). The importance of degradation of fatty acids and several aromatic compounds through central and peripheral pathways also suggests a degradation of the mucilage/biofilm interface. The release of the bound Ca^{2+} ions and carboxyl groups through degradation by aerobic respiration (Breitbart *et al.,* 2009) or consortia between sulfate reducers and fermenters (Dupraz *et al.,* 2009) can also promote mineralization independently of the light/oxygen conditions, which could explain the low rates of dark calcification sometimes observed (Borowitzka, 1987; Krumbein and Larkum, 1987). This accessory role of precipitation should be most prevalent in the space between algal cells and between these cells and the substratum, in which the influence of the coralline algae would be lessened. This collective role would explain the selective nature of some of the microbes associated with this holobiont. *Alphaproteobacteria* could also be responsible for potassium cycling and iron inputs together with *Bacteroidetes* and *Gammaproteobacteria*. *Archaea* input inorganic sulphur into the system but secrete organic acids, possibly hindering carbonate deposition.

Rhodoliths are the major dissolved carbon biofactories
Notably, the rhodolith holobiont photosynthetic capacity measured in this study via a PAM-based analysis showed high photosynthesis rates for Abrolhos rhodoliths ($52.16\,\mu mol\,carbon\,m^{-2}\,s^{-1}$) when compared with other crustose coralline algae, exemplified by *Phymatolithon foecundum* (45.2–66.9), *Phymatolithon tenue* (42.5–47.2) and *Mesophyllum engelhartii* (9.4–17.9) (Table 1) (Roberts *et al.,* 2002; Schwarz *et al.,* 2005). Nevertheless, the gross photosynthetic rate of $27.03\,g\,C\,m^{-2}$ per day calculated for the rhodolith beds was far below the previous values of 462 and $2062\,mg\,C\,m^{-2}$ per day for coastal and open ocean mesotrophic phytoplankton, respectively (Liu *et al.,* 1997; Morán *et al.,* 2002). These data may suggest that the rhodoliths also function as a heterotrophic system because of their large associated fauna, but that part of the fixed carbon is released as DOC. We calculated a rate of $3.58\,\mu mol\,C\,h\,dm^{-2}$ organic carbon released in the same range found for crustose coralline algae in Moorea, French Polynesia. On the basis of the $20\,902\,km^2$ of bank extension determined previously (Amado-Filho *et al.,* 2012) and the photosynthetic rates calculated here, the estimated total photosynthetic activity for the Abrolhos Bank is calculated to be 56.5×10^4 tons C per day. This estimate may illustrate the great importance of the Abrolhos rhodolith beds for DOC production in the South Atlantic Ocean.

Conclusion

The present study extends the previous studies on rhodoliths (Amado-Filho *et al.,* 2012), exploring the possible roles of microbes in the structure and function of rhodoliths, as well as the systemic roles of rhodoliths in the production of DOC. Calcifying algae have a significant role in the ocean carbon cycle, not only in the deposition of calcium carbonate but also in their photosynthetic capacity. Future studies utilizing metatranscriptomics (Khodadad and Foster, 2012), stable isotopes (Breitbart *et al.,* 2009) or microelectrodes (Visscher *et al.,* 1998) could extend these observations and shed new light on the biology of rhodoliths. Our first attempt to characterize the microbiome of the rhodoliths allowed us to determine the major microbial components of the rhodolith holobiont. The impressively homogeneous bacterial contribution among rhodolith replicates, coupled with the increased representation of pathways associated with aromatic compounds, fatty acids and

secondary metabolism, suggests an important chemically mediated interaction within the rhodolith holobiont. We propose that the rhodolith microbial guilds, based on their extended metabolic capacity, have important roles in the rhodolith holobiont functioning—for example, in biomineralization.

Conflict of Interest

The authors declare no conflict of interest.

Acknowledgements

We acknowledge SISBIOTA CNPq/FAPES, FAPERJ, CNPq and CAPES for funding. We also acknowledge the Project for the International Research Center for Infectious Diseases, Research Institute for Microbial Diseases, Osaka University, from the Ministry of Education, Science, Sports, Culture, and Technology, Japan. FT. Giselle Cavalcanti would like to thank the CNPq for research and PhD fellowships. This paper is part of the DSc requirements for Giselle da Silva Cavalcanti in the Biodiversity and Evolutionary Biology Graduate Program of the Federal University of Rio de Janeiro.

References

Amado-Filho GM, Moura RL, Bastos AC, Salgado LT, Sumida PY, Guth AZ *et al.* (2012). Rhodolith beds are major CaCO3 bio-factories in the tropical South West Atlantic. *PLoS One* **7**: e35171.

Bahia RG, Abrantes DP, Brasileiro PS, Pereira GH, Amado GM. (2010). Rhodolith bed structure along a depth gradient on the northern coast of Bahia state, Brazil. *Braz J Oceanogr* **58**: 323–337.

Barbera C, Bordehore C, Borg JA, Glemarec M, Grall J, Hall-Spencer JM *et al.* (2003). Conservation and management of northeast Atlantic and Mediterranean maerl beds. *Aquat Conserv* **13**: S65–S76.

Barott KL, Rodriguez-Brito B, Janouškovec J, Marhaver KL, Smith JE, Keeling P *et al.* (2011). Microbial diversity associated with four functional groups of benthic reef algae and the reef-building coral Montastraea annularis. *Environ Microbiol* **13**: 1192–1204.

Barott KL, Rohwer FL. (2012). Unseen players shape benthic competition on coral reefs. *Trends Microbiol* **20**: 621–628.

Bastos AC, Moura RL, Amado-Filho GM, D'Agostini DP, Secchin NA, Francini-Filho RB *et al.* (2013). Buracas: novel and unusual sinkhole-like features in the Abrolhos Bank. *Cont Shelf Res* (in press).

Beer S, Axelsson L. (2004). Limitations in the use of PAM fluorometry for measuring photosynthetic rates of macroalgae at high irradiances. *Eur J Phycol* **39**: 1–7.

Borowitzka MA. (1987). Calcification in Algae—mechanisms and the role of metabolism. *Crit Rev Plant Sci* **6**: 1–45.

Breitbart M, Hoare A, Nitti A, Siefert J, Haynes M, Dinsdale E *et al.* (2009). Metagenomic and stable isotopic analyses of modern freshwater microbialites in Cuatro Cienegas, Mexico. *Environ Microbiol* **11**: 16–34.

Burke C, Thomas T, Lewis M, Steinberg P, Kjelleberg S. (2011). Composition, uniqueness and variability of the epiphytic bacterial community of the green alga Ulva australis. *ISME J* **5**: 590–600.

Cavalcanti GS, Gregoracci GB, Longo LL, Bastos AC, Ferreira CM, Francini-Filho RB *et al.* (2013). Sinkhole-like structures as bioproductivity hotspots in the Abrolhos Bank. *Continental Shelf Research* (in press).

Dias GTM. (2001). Granulados bioclásticos—algas calcárias. *BrazJ Geophys* **18**: 307–308.

Dupraz C, Visscher PT. (2005). Microbial lithification in marine stromatolites and hypersaline mats. *Trens Microbiol* **13**: 429–438.

Dupraz C, Reid RP, Braissant O, Decho AW, Norman RS, Visscher PT. (2009). Processes of carbonate precipitation in modern microbial mats. *Earth-Sci Rev* **96**: 141–162.

Figueiredo MADO, Menezes KSD, Costa-paiva EM, Paiva PC, Ventura CRR. (2007). Experimental evaluation of rhodoliths as living substrata for infauna at the Abrolhos Bank, Brazil. *Cienc Mar* **33**: 427–440.

Foster MS. (2001). Rodotlihs: between rocks and soft places. *J Phycol* **37**: 659–667.

Garcia GD, Gregoracci GB, de OSE, Meirelles PM, Silva GG, Edwards R *et al.* (2013). Metagenomic analysis of healthy and white plague-affected *Mussismilia braziliensis* Corals. *Microb Ecol* **65**: 1076–1086.

Hollants J, Leliaert F, De Clerck O, Willems A. (2012). What we can learn from sushi: a review on seaweed-bacterial associations. *Fems Microbiol Ecol* **83**: 1–16.

Kamenos NA, Moore PG, Hall-Spencer JM. (2004). Maerl grounds provide both refuge and high growth potential for juvenile queen scallops (*Aequipecten opercularis* L.). *Mar Ecol* **313**: 241–254.

Khodadad CLM, Foster JS. (2012). Metagenomic and metabolic profiling of nonlithifying and lithifying stromatolitic mats of Highborne Cay, The Bahamas. *PLoS One 7.*

Krumbein MA, Larkum AWD. (1987). Calcification in algae: mechanisms and the role of metabolism. *Crit Rev Plant Sci* **6**: 1–45.

Liu H, Nolla HA, Campbell L. (1997). Prochlorococcus growth rate and contribution to primary production in the equatorial and subtropical North Pacific Ocean. *Aquat Microb Ecol* **12**: 39–49.

Maxwell K, Johnson GN. (2000). Chlorophyll fluorescence—a practical guide. *J Exp Bot* **51**: 659–668.

Meyer F, Paarmann D, D'Souza M, Olson R, Glass EM, Kubal M *et al.* (2008). The metagenomics RAST server—a public resource for the automatic phylogenetic and functional analysis of metagenomes. *BMC Bioinformatics* **9**: 386.

Morán XAG, Estrada M, Gasol JM, Pedrós-Alió C. (2002). Dissolved primary production and the strength of phytoplankton- bacterioplankton coupling in contrasting marine regions. *Microbial Ecol* **44**: 217–223.

Nelson WA. (2009). Calcified macroalgae—critical to coastal ecosystems and vulnerable to change: a review. *Mar Freshwater Res* **60**: 787–801.

Ovalle ARC, Rezende CE, Carvalho CEV, Jennerjahn TC, Ittekkot V. (1999). Biogeochemical characteristics of coastal waters adjacent to small river-mangrove systems, East Brazil. *Geo-Mar Lett* **19**: 179–185.

Overbeek R, Begley T, Butler RM, Choudhuri JV, Chuang HY, Cohoon M *et al.* (2005). The subsystems approach to genome annotation and its use in the project to annotate 1000 genomes. *Nucleic Acids Res* **33**: 5691–5702.

Parks DH, Beiko RG. (2010). Identifying biologically relevant differences between metagenomic communities *Bioinformatics* **26**: 715–721.

Reshef L, Koren O, Loya Y, Zilber-Rosenberg I, Rosenberg E. (2006). The coral probiotic hypothesis. *Environ Microbiol* **8**: 2068–2073.

Riul P, Lacouth P, Pagliosa PR, Christoffersen ML, Horta PA. (2009). Rhodolith beds at the easternmost extreme of South America: community structure of an endangered environment. *Aquat Bot* **90**: 315–320.

Roberts RD, Kuhl M, Glud RN, Rysgaard S. (2002). Primary production of crustose coralline red algae in a high Arctic fjord. *J Phycol* **38**: 273–283.

Rohwer F, Seguritan V, Azam F, Knowlton N. (2002). Diversity and distribution of coral-associated bacteria. *Mar Ecol Prog Ser* **243**: 1–10.

Rosenberg E, Koren O, Reshef L, Efrony R, Zilber-Rosenberg I. (2007). The role of microorganisms in coral health, disease and evolution. *Nat Rev Microbiol* **5**: 355–362.

Rosenberg E, Zilber-Rosenberg I. (2011). Symbiosis and development: the hologenome concept. *Birth Defects Res C Embryo Today* **93**: 56–66.

Schereiber U, Schiliwa U, Bilger W. (1966). Continuous recording of photochemical and non-photochemical chlorophyll fluorescence quenching with a new type of modulation fluorometer. *Photosynth Res* **10**: 51–62.

Schwarz AM, Hawes I, Andrew N, Mercer S, Cummings V, Thrush S. (2005). Primary production potential of non-geniculate coralline algae at Cape Evans, Ross Sea, Antarctica. *Mar Ecol Prog Ser* **294**: 131–140.

Steller DL, Riosmena-Rodriiguez R, Foster MS, Roberts CA. (2003). Rhodolith bed diversity in the Gulf of California: the importance of rhodolith structure and consequences of disturbance. *Aquat Conserv* **13**: S5–S20.

Visscher PT, Reid RP, Bebout BM, Hoeft SE, Macintyre IG, Thompson JA. (1998). Formation of lithified micritic laminae in modern marine stromatolites (Bahamas): The role of sulfur cycling. *Am Mineral* **83**: 1482–1493.

Wahl M, Goecke F, Labes A, Dobretsov S, Weinberger F. (2012). The second skin: ecological role of epibiotic biofilms on marine organisms. *Front Microbiol* **3.**

Webster NS, Cobb RE, Soo R, Anthony SL, Battershill CN, Whalan S *et al.* (2011). Bacterial community dynamics in the marine sponge rhopaloeides odorabile under *in situ* and *ex situ* cultivation. *Mar Biotechnol* **13**: 296–304.

Whalan S, Webster NS, Negri AP. (2012). Crustose coralline algae and a cnidarian neuropeptide trigger larval settlement in two coral reef sponges. *PLoS One* **7**: e30386.

Wilson S, Blake C, Berges JA, Maggs CA. (2004). Environmental tolerances of free-living coralline algae (maerl): implications for European marine conservation *Biol Conserv* **120**: 279–289.

Supplementary Information accompanies this paper on The ISME Journal website (http://www.nature.com/ismej)